

## Journal Pre-proofs

Oxygen vacancy-enriched  $V_2O_5 \cdot nH_2O$  nanofibers ink for universal substrates-tolerant and multi means-integratable  $NH_3$  sensing

Xi Xia Xing, Xin Hua Zhao, Zhen Xu Li, Ling Ling Du, Chen Wang, Dong Liang Feng, Dong Sheng Geng, Robert Bogdanowicz, Dach i Yang

PII: S1385-8947(23)05964-8  
DOI: <https://doi.org/10.1016/j.cej.2023.147233>  
Reference: CEJ 147233

To appear in: *Chemical Engineering Journal*

Received Date: 16 July 2023  
Revised Date: 22 September 2023  
Accepted Date: 7 November 2023

Please cite this article as: X. Xing, X. Zhao, Z. Li, L. Du, C. Wang, D. Feng, D. Geng, R. Bogdanowicz, D. Yang, Oxygen vacancy-enriched  $V_2O_5 \cdot nH_2O$  nanofibers ink for universal substrates-tolerant and multi means-integratable  $NH_3$  sensing, *Chemical Engineering Journal* (2023), doi: <https://doi.org/10.1016/j.cej.2023.147233>

This is a PDF file of an article that has undergone enhancements after acceptance, such as the addition of a cover page and metadata, and formatting for readability, but it is not yet the definitive version of record. This version will undergo additional copyediting, typesetting and review before it is published in its final form, but we are providing this version to give early visibility of the article. Please note that, during the production process, errors may be discovered which could affect the content, and all legal disclaimers that apply to the journal pertain.



# 1 Oxygen Vacancy-enriched $V_2O_5 \cdot nH_2O$ Nanofibers Ink for Universal 2 Substrates-tolerant and Multi Means-integratable $NH_3$ Sensing

3 Xiaxia Xing <sup>a</sup>, Xinhua Zhao <sup>a</sup>, Zhenxu Li <sup>a</sup>, Lingling Du <sup>a</sup>, Chen Wang <sup>a</sup>, Dongliang Feng <sup>a</sup>,  
4 Dongsheng Geng <sup>b</sup>, Robert Bogdanowicz <sup>c</sup>, Dachi Yang <sup>a,\*</sup>

5

6 <sup>a</sup> Tianjin Key Laboratory of Optoelectronic Sensor and Sensing Network Technology,  
7 Engineering Research Center of Thin Film Optoelectronics Technology, Ministry of  
8 Education and Department of Electronics, College of Electronic Information and Optical  
9 Engineering, Nankai University, Tianjin 300350, P. R. China

10 E-mail: yangdachi@nankai.edu.cn

11 <sup>b</sup> School of Materials Science and Engineering, University of Science and Technology  
12 Beijing, Beijing, 100083, P. R. China

13 <sup>c</sup> Department of Metrology and Optoelectronics, Faculty of Electronics,  
14 Telecommunications and Informatics, Gdansk University of Technology, 11/12G.  
15 Narutowicza St., 80-233 Gdansk, Poland

16

17 **Abstract** : Universal substrates-tolerant and multi means-integratable ammonia ( $NH_3$ )  
18 sensing is highly desired in future Internet of Things in environmental monitoring, food security  
19 and early diagnosis of human diseases, however, is still less than satisfactory. Here, an oxygen  
20 vacancy-governed  $NH_3$  sensing has been developed with  $V_2O_5 \cdot nH_2O$  nanofibers (NFs) ink, via  
21 combined thermal decomposition of ammonium metavanadate and dilution. As-obtained  $NH_3$   
22 sensing ink takes on red colloids, in which the  $V_2O_5 \cdot nH_2O$  NFs around 14 nm in diameter are  
23 interconnected. Beneficially, the fabric fiber decorated with  $V_2O_5 \cdot nH_2O$  NFs ink displays  
24 excellent selectivity and ppb-concentration detection limit. Remarkably,  $V_2O_5 \cdot nH_2O$  NFs ink  
25 is integrated over “hard” and “flexible” substrates such as glass, wood, paper, leaf and fabric  
26 with excellent tolerance by multi-integratable means such as writing, dipping and sewing.  
27 Theoretically, such  $NH_3$  sensing is interpreted that the bonding between  $V_2O_5$  NFs and  $H_2O$   
28 modulates oxygen vacancy and thus adsorption sites, and the incorporation between crystal  
29 water and free one contributes to stable ink. Practically, A sensing device built with  
30  $V_2O_5 \cdot 3.1H_2O$  NFs ink has been simulated to communicate with a smartphone with reliable  $NH_3$   
31 sensing.

32 **Keywords:** Oxygen vacancy;  $V_2O_5 \cdot nH_2O$  nanofibers sensing ink; Universal substrates-  
33 tolerant; Multi means-integratable; Ammonia sensing

34

## 35 1. Introduction

36 Ammonia ( $\text{NH}_3$ ), as a promising energy carrier [1, 2], may damage human organs if the long-  
37 term exposure to  $\text{NH}_3$  is larger than 25 ppm due to its corrosive and toxic nature [3, 4]. Instead,  
38  $\text{NH}_3$  may serve as a tracer of food spoilage [5] and an exhaled biomarker of impaired kidney  
39 [6] and liver function. As such,  $\text{NH}_3$  sensing is potentially utilized in intelligent environmental  
40 monitoring, food security and early diagnosis of human diseases, which is simultaneously  
41 required with excellent selectivity and stability, and ppb-level detection limit. Generally, a  
42 universal substrates-tolerant and multi means-integratable  $\text{NH}_3$  sensing may contribute to  
43 intelligent monitoring in the upcoming Internet of Things, although great progress has been  
44 made, it needs further exploring.

45 Actually, an  $\text{NH}_3$  sensing material with modulated sensing performance plays a crucial  
46 role in the compatible integration over universal substrates by available means. As the  $\text{NH}_3$   
47 sensing materials, semiconducting metal oxides (SMOs) have been widely investigated [7-9],  
48 however, their challenging issues may limit their future applications. Firstly, oxygen vacancy  
49 may contribute to gas sensing of SMOs materials. Theoretically, the reaction between reducing  
50 gas such as  $\text{NH}_3$  and ionized oxygen species would be boosted due to the enhanced adsorption  
51 of  $\text{O}_2$  on oxygen vacancy [10, 11]. Accordingly, the means that can generate more oxygen  
52 vacancies such as  $\text{H}_2$  plasma treatment [12], doping [13] and annealing [10, 11] have been  
53 utilized to improve the sensing performance, however, the strategies needs further developing.  
54 Secondly, the nano/micro-structured  $\text{NH}_3$  sensing SMOs are usually endowed with powder  
55 form, and their suspension in an aqueous solution may agglomerate and peel off the utilized  
56 substrate [14, 15]. Even being temporarily integrated, further mechanical manipulation may  
57 also cause similar peeling off [16]. Thirdly, the tolerance of the sensing materials to universal  
58 substrates by facially integrating means is still less than satisfactory. Conductive polymers  
59 (CPs) as  $\text{NH}_3$  sensing materials have been integrated over “hard” substrates such as glass [17]  
60 and ceramic [18] and “flexible” substrates such as polyethylene terephthalate (PET) [19] and  
61 paper [20]. Nevertheless, the substrates are still limited and their available integratable means  
62 require either complicated procedures or proficient technicians [6, 19]. Ideally, a  $\text{NH}_3$  sensing  
63 material is tolerant to various substrates by multi-integratable means and its sensing  
64 performance can be improved by an ingenious strategy, however, little has been reported so far.

65  $\text{V}_2\text{O}_5$  as a transition metal oxide presents unique electrical and sensing performance [21],  
66 in which vanadium ions ( $\text{V}^{5+}$ ) with an oxidation state generate the active sites for adsorbing  
67 gaseous molecules and catalyze reactions [22]. Compared with crystalline  $\text{V}_2\text{O}_5$ ,  $\text{V}_2\text{O}_5 \cdot n\text{H}_2\text{O}$   
68 has been investigated with a low crystallization, which is subjected to less mechanical stress  
69 and thus offers more active sites than their crystalline counterparts during reaction [23]. Notably,  
70 the presence of crystal water has been reported to boost the electrochemical reaction kinetics  
71 [24]. Being inspired, an oxygen vacancy-enriched  $\text{V}_2\text{O}_5 \cdot n\text{H}_2\text{O}$  nanofibers (NFs) ink with a sol  
72 form in this study has been developed for universal substrates-tolerant and multi means-  
73 integratable  $\text{NH}_3$  sensing at room temperature. As characterized, the  $\text{V}_2\text{O}_5 \cdot n\text{H}_2\text{O}$  NFs of ~14  
74 nm in diameter are interconnected to form red and highly dispersed ink with a zeta potential of  
75 ~ 38.8 mV. Beneficially, the response of diluted  $\text{V}_2\text{O}_5 \cdot 3.1\text{H}_2\text{O}$  NFs fabric to 10 ppm  $\text{NH}_3$  have  
76 been improved ( $S = 17.8\%$ ) compared with that of pristine one ( $S = 8.6\%$ ). Furthermore, the  
77 diluted  $\text{V}_2\text{O}_5 \cdot 3.1\text{H}_2\text{O}$  NFs fabric fiber shows 100 ppb detection limit of  $\text{NH}_3$  and excellent  
78 selectivity. Remarkably, the  $\text{V}_2\text{O}_5 \cdot n\text{H}_2\text{O}$  NFs ink has been integrated on various substrates such  
79 as ceramics, glass, wood, paper, fabric and leaf, by which multi-integratable means of writing,  
80 dipping and sewing have been applied. Such sensing ink would contribute to the diversification  
81 of  $\text{NH}_3$  sensors in future intelligent sensing.

82



## 83 2. Experimental section

### 84 2.1 Synthesis of $V_2O_5 \cdot 2.3H_2O$ NFs ink [25]

85 Firstly, 1 g ammonium metavanadate ( $NH_4VO_3$ ) was ground with deionized (D.I.) water, and  
86 then the fluid was mixed with 10 mL of 1M HCl under continuous stirring. Secondly, when the  
87 suspension turns red, D.I. water was added to make the total volume of 20 mL, the supernatant  
88 was removed after precipitation. Thirdly, the red precipitate was dispersed into 80-90 °C hot  
89 water to a total volume of 20 mL, the supernatant was removed after stirring and precipitating.  
90 Finally, the dark red  $V_2O_5 \cdot 2.3H_2O$  NFs dispersions were filled with 80-90 °C hot water to a  
91 total volume of 40 mL for the subsequent utilization.

### 92 2.2 Synthesis of sensing fabrics and fabrics fiber integrating $V_2O_5 \cdot nH_2O$ NFs ink

93 Synthesis of  $V_2O_5 \cdot nH_2O$  NFs fabrics is briefly described as follows. Initially, 0.5 mL, 2 mL  
94 and 5 mL of the above synthesized  $V_2O_5 \cdot 2.3H_2O$  NFs ink were ultrasonically dispersed in 10  
95 mL D.I. water, respectively. Correspondingly, they are denoted as ink-0.5, ink-2 and ink-5 in  
96 Fig. 3a, respectively. Secondly, the rectangular polyester fabric (2 cm×0.5 cm) and fabric fiber  
97 (Diameter: ~ 207 μm, Length: ~ 2 cm) was immersed in the above synthesized  $V_2O_5 \cdot nH_2O$  NFs  
98 dispersion for 1 min. Finally, the  $V_2O_5 \cdot nH_2O$  NFs fabrics and fabric fiber were dried at room  
99 temperature. In the same way, the sensing ink was integrated over the PET and paper in Fig. 5e.  
100 It should be noted that 2 mL of the pristine  $V_2O_5 \cdot 2.3H_2O$  NFs ultrasonically dispersed in 10  
101 mL D.I. water was defined as diluted  $V_2O_5 \cdot 3.1H_2O$  NFs ink, which was taken as an example  
102 for deep investigation.

### 103 2.3 Synthesis of $V_2O_5 \cdot 2.3H_2O$ NFs aerogel and powder, and $V_2O_5$ NFs powder

104 The  $V_2O_5 \cdot 2.3H_2O$  NFs ink was firstly frozen at -18 °C and then lyophilized at -51 °C in a  
105 freeze-drier (FD-1A-50, Henan Brothers Instrument and Equipment Co., Ltd., China) to obtain  
106  $V_2O_5 \cdot 2.3H_2O$  NFs aerogel. The  $V_2O_5 \cdot 2.3H_2O$  NFs aerogel was grounded using an agate mortar  
107 to obtain  $V_2O_5 \cdot 2.3H_2O$  NFs powder, its resistivity was tested under various pressures (2-30  
108 MPa) in Fig. S1, in which the resistivity mean is ~ 7823 Ωcm. The  $V_2O_5 \cdot 2.3H_2O$  NFs powder  
109 was annealed in air at 600 °C for 2 h to remove the crystal water, then the  $V_2O_5$  NFs powder  
110 was collected.

### 111 2.4 Characterization

112 The samples were characterized by field emission scanning electron microscopy (FE-SEM,  
113 JSM-7800) with energy dispersive X-ray spectroscopy (EDS, Oxford), transmission electron  
114 microscopy (TEM, JEM-2200FS), X-ray diffraction (XRD, Rigaku Smart Lab 3kW) using Cu  
115  $K\alpha$  radiation, Raman spectra (SR-500I-A, a wavelength of 532 nm as the excitation),  
116 Ultraviolet-visible diffuse reflectance spectra (Shimadzu UV-3600), Mott-Schottky test  
117 (electrochemistry workstation VersaSTAT 4, AMETEK Princeton), thermogravimetric  
118 analysis (TGA) (Netzsch STA449F5 instrument, temperature range 30-600 °C, heating rate  
119 10 °C/min, in nitrogen atmosphere), Automatic powder resistivity tester (ST2742B), Zeta  
120 potential analyzer (Malvern Zetasizer Nano ZS ZEN3600, UK), electron paramagnetic  
121 resonance (EPR) spectroscopy (Bruker EMXPLUS) and X-ray photoelectron spectroscopy  
122 (XPS, Thermo Scientific ESCALAB 250Xi). The XPS spectra on binding energies of various  
123 elements have been calibrated with C 1s at 284.8 eV.

### 124 2.5 Gas sensing measurement

125 The gas sensing was tested at room temperature (RT, ~ 25 °C) in air atmosphere. In detail, the  
 126 two ends of fabric were connected to the Data Acquisition System (KEITHLEY 2701) by two  
 127 gold clamps, which were placed in a homemade test chamber of 18 L with two air fans and a  
 128 vaporizer. Notably, the NH<sub>3</sub> sensing is *in-situ* detection directly without other electrodes.  
 129 Additionally, the gaseous and dry NH<sub>3</sub> with high-purity was adopted. The calculation of NH<sub>3</sub>  
 130 concentration is conducted by the gas distribution formula (equation 1), in which C (ppm) and  
 131  $\varphi$  represent the target gas concentration and volume fraction, respectively, and V<sub>1</sub> (mL) and V<sub>2</sub>  
 132 (mL) are denoted as the volume of target gas and testing chamber (V<sub>2</sub> = 18 L). The sensing  
 133 response is expressed by  $S = (R_g/R_a - 1) * 100\%$ , of which R<sub>a</sub> and R<sub>g</sub> are the resistances in the air  
 134 and target gas, respectively. The response/recovery time is defined as the time taken by the  
 135 sensor to reach 90% of the final steady-state resistance after injecting or switching off the target  
 136 gas.

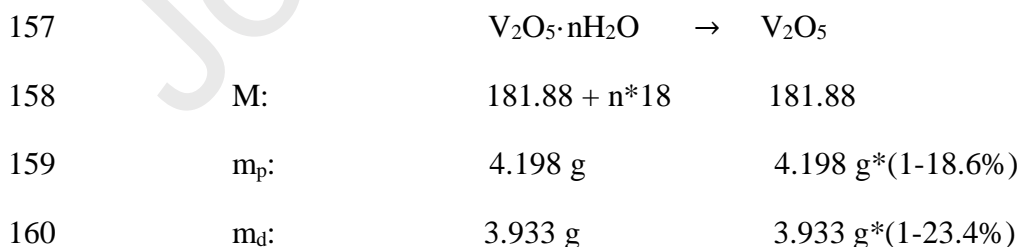
$$137 \quad V_1 = \frac{V_2 \times C}{\varphi} \times 10^{-6} \quad (1)$$

138

### 139 3. Results and Discussion

#### 140 3.1. Synthesis and characterization

141 In Fig. 1a, the pristine V<sub>2</sub>O<sub>5</sub>·nH<sub>2</sub>O NFs ink was diluted and integrated over fabrics, and the  
 142 synthetic details of pristine V<sub>2</sub>O<sub>5</sub>·nH<sub>2</sub>O NFs ink were provided in above experimental section.  
 143 Meanwhile, the three-dimensional (3D) crystal structure of V<sub>2</sub>O<sub>5</sub>·nH<sub>2</sub>O NFs was simulated by  
 144 Visualization for Electronic and STructural Analysis (VESTA) [26]. Also, the X-ray  
 145 diffractions (XRD) of pristine and diluted V<sub>2</sub>O<sub>5</sub>·nH<sub>2</sub>O NFs were conducted (Fig. S2a) with the  
 146 diffractive peak of V<sub>2</sub>O<sub>5</sub>·nH<sub>2</sub>O at ~ 10° [27]. Meanwhile, the crystal water was removed by  
 147 annealing the pristine V<sub>2</sub>O<sub>5</sub>·nH<sub>2</sub>O NFs, and was then confirmed as the V<sub>2</sub>O<sub>5</sub> (PDF#89-0612) in  
 148 Fig. S2b. Further, Raman spectra of pristine V<sub>2</sub>O<sub>5</sub>·nH<sub>2</sub>O NFs (Fig. S2c) show the V-O Raman  
 149 scattering peaks with the orthorhombic crystalline [28]. Remarkably, the thermogravimetric  
 150 analysis (TGA) was carried out to determine the “n” value in V<sub>2</sub>O<sub>5</sub>·nH<sub>2</sub>O NFs. In Fig. 1b,  
 151 weight loss of 23.4% and 18.6% occur at 100 - 600 °C, which is attributed to the loss of crystal  
 152 water, and the “n” values corresponding to diluted and pristine V<sub>2</sub>O<sub>5</sub>·nH<sub>2</sub>O NFs are 3.1 and 2.3,  
 153 respectively. Specifically, the detailed calculation of “n” value in V<sub>2</sub>O<sub>5</sub>·nH<sub>2</sub>O is described as  
 154 follows. M, m<sub>p</sub> and m<sub>d</sub> represent relative molecular mass, mass of pristine V<sub>2</sub>O<sub>5</sub>·nH<sub>2</sub>O NFs and  
 155 mass of diluted one, respectively. Therefore, the “n” values corresponding to the diluted and  
 156 pristine ones are calculated by the bellow proportional formula of the chemical equation.



161 In Fig. 1c, V<sub>2</sub>O<sub>5</sub>·3.1H<sub>2</sub>O NFs ink is observed dense and overlapped in a lower  
 162 magnification with scanning electron microscopy (SEM). While in a closer observation under  
 163 transmission electron microscopy (TEM), the diameter of V<sub>2</sub>O<sub>5</sub>·nH<sub>2</sub>O NFs in Fig. 1d is  
 164 measured ~ 14 nm (Fig. S3). Moreover, the high-resolution TEM (HR-TEM) image and  
 165 selected area electron diffraction (SAED) pattern in Fig. 1f and Fig. S4 show the (102) plane of

166  $V_2O_5$  (PDF#89-0612). Further, the elemental mappings under TEM (Fig. S5) verified the  
 167 existence of V and O elements, and the diameter of the fabric fiber integrated with diluted  
 168  $V_2O_5 \cdot 3.1H_2O$  NFs ink was measured  $\sim 207 \mu m$  in Fig. 1g<sub>1</sub>. By comparing with the shape of  
 169 pristine fabric fiber in Fig. 1h<sub>1</sub>, the flake shape in Fig. 1g<sub>2</sub> reveals that the  $V_2O_5 \cdot 3.1H_2O$  NFs  
 170 ink has been integrated over fabrics. Interestingly, the Tyndall effects of pristine and various  
 171 diluted ink were compared in Fig. S6, the dispersibility of pristine  $V_2O_5 \cdot 2.3H_2O$  NFs ink can  
 172 be improved via dilution.

### 173 3.2. The stable $V_2O_5 \cdot nH_2O$ NFs ink for dilution-modulated $NH_3$ sensing

174 To get insight into the role of water in  $V_2O_5 \cdot nH_2O$  NFs ink, the free water was initially removed  
 175 by freezing and drying  $V_2O_5 \cdot 2.3H_2O$  NFs ink, and then the lyophilized ones were annealed to  
 176 remove crystal water and obtain  $V_2O_5$  for subsequent comparison. In Fig. S7, the color of  
 177  $V_2O_5 \cdot 2.3H_2O$  NFs powder changed from its pristine dark red to orange after annealing. The  
 178  $V_2O_5$  and  $V_2O_5 \cdot 2.3H_2O$  NFs powder were ultrasonically dispersed into D.I. water and pure  
 179 ethanol, respectively. Correspondingly, various dispersions were dripped over interdigital  
 180 electrodes in Fig. 2d for comparing their  $NH_3$  sensing performance, and the real-time resistance  
 181 curves were shown in Fig. 2a.

182 In Fig. 2b-c, the  $V_2O_5 \cdot 2.3H_2O$  NFs exhibit a higher response to 10 ppm  $NH_3$  than that of  
 183  $V_2O_5$  NFs in both water and pure ethanol solvent, revealing the crystal water-boosted  $NH_3$   
 184 sensing. Actually, water solvent may contribute to lower baseline resistance in both  $V_2O_5$  and  
 185  $V_2O_5 \cdot nH_2O$  NFs (Fig. 2c). Further, free water is required in preparing  $V_2O_5 \cdot nH_2O$  NFs ink in  
 186 Fig. 2e. Otherwise, uneven and unstable dispersion can be obtained. Meanwhile, the  
 187  $V_2O_5 \cdot 2.3H_2O$  NFs ink and ethanol dispersion were dipped over fabric in Fig. 2d<sub>1</sub>. In Fig. S8,  
 188 the resistance value of  $V_2O_5 \cdot 2.3H_2O$  NFs ink fabric is  $\sim 0.49 M\Omega$ , however, the one with  
 189 ethanol dispersion is larger than  $20 M\Omega$ , which reveals that the uniform and stable  $V_2O_5 \cdot 2.3H_2O$   
 190 NFs ink contribute to integrating conductive fabric. Notably, if one deliberately removed the  
 191 crystal water in  $V_2O_5 \cdot 2.3H_2O$  NFs or replaced the dispersion medium from water to pure  
 192 ethanol, the dispersed phase is obviously separated from dispersion medium (Fig. 2e), rather  
 193 than obtaining stable ink. As such, the incorporation of crystal water bonded by  $V_2O_5$  with free  
 194 water in the dispersion medium plays a pivotal role in the formation of sensing ink.

195 The diluted  $V_2O_5 \cdot 3.1H_2O$  and pristine  $V_2O_5 \cdot 2.3H_2O$  NFs inks were observed with the  
 196 variation of Tyndall effect in Fig. 2f and g, in which the light path penetrates after diluting with  
 197 high dispersibility of colloid [29]. Meanwhile, the simulated 3D crystalline structures with  
 198 various oxygen vacancies of diluted and pristine  $V_2O_5 \cdot nH_2O$  NFs are shown in Fig. 2f<sub>1</sub> and g<sub>1</sub>,  
 199 respectively. With the pristine  $V_2O_5 \cdot 2.3H_2O$  NFs ink for comparisons, the diluted  $V_2O_5 \cdot 3.1H_2O$   
 200 NFs ink was integrated over the fabric (2 cm $\times$ 0.5 cm) and the fabric fiber (Diameter:  $\sim 207 \mu m$ ,  
 201 Length:  $\sim 2$  cm), respectively. In the photographs of Fig. 2f and g, the color of diluted  
 202  $V_2O_5 \cdot 3.1H_2O$  NFs fabrics was seen lighter than that of pristine  $V_2O_5 \cdot 2.3H_2O$  ones. To further  
 203 gain insight into the role of dilution, the  $NH_3$  sensing performance of the above integrated  
 204 various pristine  $V_2O_5 \cdot 2.3H_2O$  and diluted  $V_2O_5 \cdot 3.1H_2O$  NFs fabric were investigated with  
 205 comparison. In Fig. 2h, the recovery speed of pristine  $V_2O_5 \cdot 2.3H_2O$  NFs fabric is improved by  
 206 both diluting and adopting the fabric fiber. Meanwhile, the responses toward 5 ppm and 25 ppm  
 207  $NH_3$  were summarized in Fig. 2i, and show that the sensing responses of diluted  $V_2O_5 \cdot 3.1H_2O$   
 208 NFs ink onto both fabric and fabric fiber are higher than those of pristine ones. Moreover, the  
 209 real-time responses to 1-50 ppm  $NH_3$  were evaluated in Fig. 2j, which further reveals the  
 210 dilution improved  $NH_3$  sensing performance.

### 211 3.3. Evaluation of the $NH_3$ sensing performance

212 The content of  $V_2O_5 \cdot nH_2O$  NFs in the sensing ink governs the  $NH_3$  sensing. In Fig. 3a, the  
 213 responses of pristine and various diluted  $V_2O_5 \cdot nH_2O$  NFs fabric to 10 ppm  $NH_3$  were evaluated,  
 214 and the  $V_2O_5 \cdot nH_2O$ -2 mL NFs fabric manifested the highest response ( $S = 17.8\%$ ) compared  
 215 with pristine ones ( $S = 8.6\%$ ), and was thus chosen for subsequent evaluation and renamed by  
 216  $V_2O_5 \cdot 3.1H_2O$  NFs fabric. The response and recovery time were evaluated to  $\sim 75$  s and 36 s  
 217 toward 1 ppm  $NH_3$  in Fig. S9, respectively. Remarkably, the flexibility of  $V_2O_5 \cdot nH_2O$  NFs  
 218 fabric was investigated by testing their responses to 1 ppm and 10 ppm  $NH_3$  upon the bending  
 219 angle at  $0^\circ$ ,  $45^\circ$ ,  $90^\circ$  and  $360^\circ$ , respectively. Excitedly, little difference was observed in Fig. 3b,  
 220 indicating excellent flexibility.

221 The stability and selectivity are crucial parameters for  $NH_3$  sensing. Remarkably, the  
 222 sensing evaluation to 5 ppm  $NH_3$  is repeated for 126 days' durations in Fig. 3c with good  
 223 stability. Furthermore, the responses of various interfering gases and 10 ppm target  $NH_3$  were  
 224 compared in Fig. 3d, revealing excellent selectivity. Meanwhile, the  $NH_3$  sensing of three  
 225  $V_2O_5 \cdot 2.3H_2O$  NFs fabrics in Fig. S10 is compared, which shows a slight variation in response  
 226 to the same concentration  $NH_3$  and takes a good consistency. Additionally, the diluted  
 227  $V_2O_5 \cdot 3.1H_2O$  NFs ink was integrated over the fabric fiber in Fig. 3e, and its low detection limit  
 228 is around 100 ppb  $NH_3$ . Towards a low  $NH_3$  concentration (e.g., 100 ppb-1 ppm), the responses  
 229 show an excellent linear relationship in Fig. 3f. While towards a high one (e.g., 1-50 ppm),  
 230 excellent repeatability is observed in Fig. 3g. As a result, the  $V_2O_5 \cdot nH_2O$  NFs fabric  
 231 simultaneously present ppb-level detection, high selectivity and stability, excellent flexibility  
 232 and low working temperature. Compared with other SMOs  $NH_3$  sensing materials in Table 1,  
 233 a gel-stated and stable ink of  $V_2O_5 \cdot nH_2O$  NFs is prepared, which can be integrated over various  
 234 "hard" and "flexible" substrates by multi-integratable means.

235 In our experiments, both temperature and humidity can influence the  $NH_3$  sensing. In Fig.  
 236 S11, the temperature-dependent sensing responses were observed to 20 ppm  $NH_3$  at  $\sim 26$ -140  
 237  $^\circ C$ , and the highest one takes place at room temperature ( $\sim 26$   $^\circ C$ ). Meanwhile, the baseline  
 238 resistance and the sensing response of  $V_2O_5 \cdot 3.1H_2O$  NFs fabric toward 5 ppm  $NH_3$  decrease  
 239 with humidity (Fig. S12), similar to previous SMOs [30] and to other humidity sensors [31].  
 240 Such a decrease in the sensing response might be interpreted that  $H_2O$  molecules occupy  
 241 adsorption sites, which weakens the reaction between  $NH_3$  and adsorbed oxygen onto the  
 242 surface of  $V_2O_5 \cdot 3.1H_2O$  NFs [32], as may be addressed by covering filter membrane [33].

### 243 3.4. The oxygen vacancy governed $NH_3$ sensing mechanism

244 We experimentally investigated the chemisorbed oxygen to understand the dilution-boosted  
 245  $NH_3$  sensing mechanism, and three characterizations on oxygen vacancy ( $V_o$ ) of diluted  
 246  $V_2O_5 \cdot 3.1H_2O$  NFs were performed with pristine  $V_2O_5 \cdot 2.3H_2O$  ones as comparison. Firstly, the  
 247 O 1s X-ray photoelectron spectroscopy (XPS) in Fig. 4a spectra were deconvoluted into three  
 248 oxygen species of  $O_I$ ,  $O_{II}$  and  $O_{III}$ , which are associated with oxygen atoms bound to metals,  
 249 defect sites with low oxygen coordination and hydroxy species, respectively. Remarkably, the  
 250 integral-area ratios of  $O_{II}$  increase from 20% of pristine  $V_2O_5 \cdot 2.3H_2O$  NFs to 52% of diluted  
 251  $V_2O_5 \cdot 3.1H_2O$  ones, indicating that the diluted  $V_2O_5 \cdot 3.1H_2O$  one possesses more oxygen  
 252 vacancies [34]. Meanwhile, the V 2p spectra in Fig. 4b correspond to the characteristics of  $V^{5+}$ ,  
 253 the discrepancy in binding energy (0.3 eV) indicates distinct electronic environments of V ions  
 254 in the pristine and diluted  $V_2O_5 \cdot nH_2O$  NFs, which might be interpreted as increased oxygen  
 255 vacancy in the diluted  $V_2O_5 \cdot 3.1H_2O$  ones [10]. Secondly, the presence of oxygen vacancy was  
 256 further studied by electron paramagnetic resonance (EPR) spectroscopic measurements in Fig.  
 257 4c and symmetrical EPR signals ( $g = 1.9612$ ) are assigned to the unpaired electrons in the  
 258 oxygen vacancy sites [10, 35]. The ESR intensity of diluted  $V_2O_5 \cdot 3.1H_2O$  NFs is higher than

259 that of pristine  $V_2O_5 \cdot 2.3H_2O$  ones, indicating dilution governed the oxygen vacancy, which  
 260 result in more chemisorbed oxygen for gas sensing. Thirdly, such result is also evidenced by  
 261 the narrower optical bandgaps ( $E_g$ ) of diluted  $V_2O_5 \cdot 3.1H_2O$  NFs (1.87 eV) than that of pristine  
 262  $V_2O_5 \cdot 2.3H_2O$  (2.19 eV) in Fig. 4d.

263 The energy-band variation of  $V_2O_5 \cdot nH_2O$  NFs was investigated for understanding the  $NH_3$   
 264 sensing mechanism. Specifically, the valence band maximum ( $E_v$ ) of the  $V_2O_5 \cdot 3.1H_2O$  NFs is  
 265 determined to  $\sim 2.4$  eV (Fig. S14). Accordingly, the conduction band minimum ( $E_c$ ) of  
 266  $V_2O_5 \cdot 3.1H_2O$  is calculated to  $\sim 0.53$  eV according to Equation (2). Usually,  $V_2O_5$  is reported  
 267 as a n-type semiconductor [36]. However, p-type sensing characteristic with increased  
 268 resistance was observed in this study (Fig. 2a and h), which is explained as follows. The  
 269  $V_2O_5 \cdot 3.1H_2O$  NFs contain abundant oxygen vacancy, which will improve chemisorption of  $O_2$   
 270 and  $H_2O$  molecule [11, 37], capture more electrons from the conduction band of  $V_2O_5 \cdot nH_2O$   
 271 NFs and thus bend upward band causing an inversion layer, therefore, the Fermi level ( $E_F$ )  
 272 located below the intrinsic level ( $E_i$ ) in Fig. 4e [38]. In the surface inversion layer, holes usually  
 273 serve as the major carriers with p-type feature, which was confirmed by Mott-Schottky with a  
 274 negative slope in Fig. 4e<sub>1</sub>.

$$275 \quad E_c = E_v - E_g \quad (2)$$

276 To understand the p-type sensing mechanism, the  $NH_3$  sensing evaluations under various  
 277 working temperatures were investigated in Fig. S11, the  $V_2O_5 \cdot 3.1H_2O$  NFs show increased  
 278 sensing resistance to 20 ppm  $NH_3$  at  $\sim 26-80$  °C and decreased ones at  $\sim 100-140$  °C. Such  
 279 phenomenon is explained as follows. At lower temperatures, the strong adsorption of  $O_2$  and  
 280  $H_2O$  molecules contribute to the formation of an inversion layer on the surface of  $V_2O_5 \cdot 3.1H_2O$   
 281 NFs, exhibiting p-type semiconductor properties [39]. With the elevating of temperature, an  
 282 inversion layer would be destroyed without sufficient  $O_2$  and  $H_2O$  molecules, n-type sensing  
 283 behavior would be seen. Further, we conducted additional comparative experiments on  $NH_3$   
 284 sensing under insufficient oxygen conditions and air atmosphere in Fig. S15, the significantly  
 285 decreased response in Fig. S15a indicates that the sufficient surface adsorption of oxygen  
 286 contributes to  $NH_3$  sensing of  $V_2O_5 \cdot 3.1H_2O$  NFs.

287 Accordingly, the  $NH_3$  sensing mechanism of  $V_2O_5 \cdot nH_2O$  NFs fabrics is interpreted as  
 288 follows. In Fig. 4f, when the pristine p-type  $V_2O_5 \cdot 2.3H_2O$  ones are exposed to  $NH_3$ , the pre-  
 289 adsorbed oxygen species ( $O_2^-$ ) and hydroxy species ( $-OH$ ) react with  $NH_3$  and release electrons  
 290 [40, 41], reducing the hole concentration and thus elevating the resistance. Similarly, the diluted  
 291  $V_2O_5 \cdot 3.1H_2O$  NFs show  $NH_3$  sensing mechanism in Fig. 4f<sub>1</sub>. However, the content of their  
 292 oxygen vacancy is significantly increased thus improved chemisorbed oxygen, and finally  
 293 present boosted  $NH_3$  sensing.

### 294 **3.5. $V_2O_5 \cdot nH_2O$ NFs ink for universal substrates-tolerant and multi means-integratable** 295 **$NH_3$ sensing and the simulation detection of $NH_3$**

296 The universal-substrates tolerance and multi-means integration of  $V_2O_5 \cdot 2.3H_2O$  NFs ink were  
 297 investigated. The tolerance has been widely examined on hard substrates such as ceramics,  
 298 stainless steel, glass and wood, and flexible ones such as Chinese “Xuan” paper, leaf, Al foil,  
 299 plastic wrap and A4 size paper in Fig. 5a. Meanwhile, the adhesive performance of the  
 300  $V_2O_5 \cdot 2.3H_2O$  NFs ink over the above substrate has been investigated in Fig. S16, one can see  
 301 that the adhesive properties depend on the substrates and the sensing ink shows a weaker  
 302 adhesion than that of commercial one on A4 paper (Fig. S17). As for the integratable means,  
 303 our  $V_2O_5 \cdot 2.3H_2O$  NFs ink can be dipped with a paintbrush to draw the school badge and the  
 304 motto of Nankai University in Fig. 5a and other “dipping-drying” approach in Fig. 5b.



305 Impressively, the  $V_2O_5 \cdot 3.1H_2O$  NFs ink can also serve as a colouring agent with color variation  
306 from white of pristine fabric fiber to orange, which can be integrated over the fabric fiber (Fig.  
307 5c), and can even be sewed on the clothes with the “NKU” pattern. Particularly, by freezing  
308 and drying, the  $V_2O_5 \cdot 3.1H_2O$  NFs ink can be transformed into lightweight aerogel, and can  
309 even stand on the tip of the reed (Fig. S18). In this case, even being storing 365 days (Fig. 5d)  
310 and 608 days (Fig. S19a), the  $V_2O_5 \cdot 3.1H_2O$  NFs ink remains excellent dispersibility and  
311 stability, which is verified by characterizing the zeta potential of  $V_2O_5 \cdot 3.1H_2O$  NFs ink to ~  
312 38.8 mV after storing 608 days (Fig. S19b).

313 As examples, the PET, Chinese “Xuan” paper and fabric integrated with  $V_2O_5 \cdot 3.1H_2O$   
314 NFs ink were examined for their  $NH_3$  sensing performance in Fig. 5e, showing substrates-  
315 dependent  $NH_3$  sensing, which may be explained that these bare and insulated substrates serve  
316 as support and don't participate electron transport. Although previous investigations (Table 1)  
317 have made great progress, our  $V_2O_5 \cdot nH_2O$  NFs ink is the one that can be simultaneously utilized  
318 for universal substrates-tolerant and multi means-integratable  $NH_3$  sensing. Practically, such  
319  $NH_3$  sensing ink enable to be integrated into the feasible substrates such as smocks, mask and  
320 food packaging bag for environmental monitoring, exhaled diagnosis of human diseases and  
321 inspection of food safety. Herein, we elaborately integrated the  $V_2O_5 \cdot 3.1H_2O$  NFs ink onto the  
322 polyethylene sample bag (4 cm×6 cm) as an example, to simulate detection of  $NH_3$ , which was  
323 read by a smartphone (Fig. 5f). Specifically, the microcontroller NodeMCU (ESP8266, 5.8  
324 cm×3.1 cm) with Wireless Fidelity (Wi-Fi) module communicate with the smartphone and  
325 perform the  $NH_3$  sensing and alarming of the device. In the supplemental video, when 10 ppm  
326  $NH_3$  was injected and the sensing voltage is lower than the alarm threshold (0.5 V), the  
327 smartphone read “ALARMING!” (Fig. 5g). Conversely, the  $NH_3$  being released with the one  
328 higher than 0.5 V, and “Monitoring” in smartphone is seen. Also, the detailed historical  
329 information can be read and recorded in Fig. 5h, which is great potential for inspection of food  
330 safety.

331

## 332 4. Conclusion

333 To summarize, an oxygen vacancy-enriched  $V_2O_5 \cdot nH_2O$  NFs ink has been developed by  
334 combining the thermal decomposition of ammonium metavanadate with subsequent dilution,  
335 for universal substrates-tolerant and multi means-integratable  $NH_3$  sensing at room temperature.  
336 Experimentally, the  $V_2O_5 \cdot nH_2O$  NFs of ~ 14 nm in diameter were observed to be interconnected,  
337 forming red colloids in an aqueous solution with high dispersibility. Theoretically, the bonding  
338 between  $V_2O_5$  NFs and  $H_2O$  governs the oxygen vacancy with improved the adsorption sites of  
339  $NH_3$ , and the incorporation between crystal water and free water contributes to stable ink.  
340 Beneficially, the diluted  $V_2O_5 \cdot 3.1H_2O$  NFs fabrics show an increased response to 10 ppm  $NH_3$   
341 ( $S = 17.8\%$ ) compared with the pristine ones ( $S = 8.6\%$ ). Also, the  $V_2O_5 \cdot nH_2O$  NFs ink fabric  
342 fiber displays excellent selectivity and ppb-level detection limit to  $NH_3$ . Remarkably,  
343  $V_2O_5 \cdot nH_2O$  NFs ink has been integrated over various substrates such as ceramics, glass, wood,  
344 paper, fabric and leaf with universal substrates-tolerance. Meanwhile, multiple strategies of  
345 writing, dipping and sewing have been adopted for integration. As an example of application,  
346 the developed oxygen vacancy-enriched  $V_2O_5 \cdot 3.1H_2O$  NFs ink has been integrated into a  
347 sensing device and communicates with a smartphone with reliable monitoring and alarming,  
348 which is potential in future intelligent sensing of Internet of Things. Future investigations are  
349 expected to be conducted on theoretical calculations and humidity-dependent  $NH_3$  sensing.

350

## 351 Declaration of Competing Interest

352 The authors declare that they have no known competing financial interests or personal  
353 relationships that could have appeared to influence the work reported in this paper.

354

## 355 Data availability

356 Data will be made available on request.

357

## 358 Acknowledgements

359 This work was financially supported by the National Natural Science Foundation of China  
360 (Grant No. 52072184) and Tianjin Research Innovation Project for Postgraduate Students  
361 (General Project, Grant No. 2022BKY035).

362

## 363 References

- 364 [1] W. Gao, J. Guo, P. Wang, Q. Wang, F. Chang, Q. Pei, W. Zhang, L. Liu, P. Chen,  
365 Production of ammonia via a chemical looping process based on metal imides as nitrogen  
366 carriers, *Nat. Energy* 3 (2018) 1067-1075.
- 367 [2] K. Nakajima, H. Toda, K. Sakata, Y. Nishibayashi, Ruthenium-catalysed oxidative  
368 conversion of ammonia into dinitrogen, *Nat. Chem.* 11 (2019) 702-709.
- 369 [3] M. Van Damme, L. Clarisse, S. Whitburn, J. Hadji-Lazaro, D. Hurtmans, C. Clerbaux,  
370 P.-F. Coheur, Industrial and agricultural ammonia point sources exposed, *Nature* 564  
371 (2018) 99-103.
- 372 [4] A.T. Güntner, M. Wied, N.J. Pineau, S.E. Pratsinis, Rapid and Selective NH<sub>3</sub> Sensing by  
373 Porous CuBr, *Adv. Sci.* 7 (2020) 1903390.
- 374 [5] Z. Ma, P. Chen, W. Cheng, K. Yan, L. Pan, Y. Shi, G. Yu, Highly Sensitive, Printable  
375 Nanostructured Conductive Polymer Wireless Sensor for Food Spoilage Detection, *Nano*  
376 *Lett.* 18 (2018) 4570-4575.
- 377 [6] H.-Y. Li, C.-S. Lee, D.H. Kim, J.-H. Lee, Flexible Room-Temperature NH<sub>3</sub> Sensor for  
378 Ultrasensitive, Selective, and Humidity-Independent Gas Detection, *ACS Appl. Mater.*  
379 *Interfaces* 10 (2018) 27858-27867.
- 380 [7] B. Yang, X. Li, W. Yuan, Z. Li, N. Lu, S. Wang, Y. Wu, S. Fan, Z. Hua, Efficient NH<sub>3</sub>  
381 Detection Based on MOS Sensors Coupled with Catalytic Conversion, *ACS Sens.* 5  
382 (2020) 1838-1848.
- 383 [8] S. Kumar, A. Singh, R. Singh, S. Singh, P. Kumar, R. Kumar, Facile h-MoO<sub>3</sub> synthesis  
384 for NH<sub>3</sub> gas sensing application at moderate operating temperature, *Sens. Actuator B*  
385 *Chem.* 325 (2020) 128974.



- 386 [9] Y.-Y. Li, J.-L. Chen, F.-L. Gong, G.-X. Jin, K.-F. Xie, X.-Y. Yang, Y.-H. Zhang, Dual  
387 functionalized Ni substitution in shuttle-like  $\text{In}_2\text{O}_3$  enabling high sensitivity  $\text{NH}_3$   
388 detection, *Appl. Surf. Sci.* 600 (2022) 154158.
- 389 [10] H. Yuan, S.A.A.A. Aljneibi, J. Yuan, Y. Wang, H. Liu, J. Fang, C. Tang, X. Yan, H. Cai,  
390 Y. Gu, S.J. Pennycook, J. Tao, D. Zhao, ZnO Nanosheets Abundant in Oxygen Vacancies  
391 Derived from Metal-Organic Frameworks for ppb-Level Gas Sensing, *Adv. Mater.* 31  
392 (2019) 1807161.
- 393 [11] G. Li, H. Zhang, L. Meng, Z. Sun, Z. Chen, X. Huang, Y. Qin, Adjustment of oxygen  
394 vacancy states in ZnO and its application in ppb-level  $\text{NO}_2$  gas sensor, *Sci. Bull.* 65 (2020)  
395 1650-1658.
- 396 [12] Z. Geng, X. Kong, W. Chen, H. Su, Y. Liu, F. Cai, G. Wang, J. Zeng, Oxygen Vacancies  
397 in ZnO Nanosheets Enhance  $\text{CO}_2$  Electrochemical Reduction to CO, *Angew. Chem. Int.*  
398 *Ed.* 57 (2018) 6054-6059.
- 399 [13] X. Wang, T. Wang, G. Si, Y. Li, S. Zhang, X. Deng, X. Xu, Oxygen vacancy defects  
400 engineering on Ce-doped  $\alpha\text{-Fe}_2\text{O}_3$  gas sensor for reducing gases, *Sens. Actuator B Chem.*  
401 302 (2020) 127165.
- 402 [14] J.H. Kim, J.H. Han, Y.C. Jung, Y.A. Kim, Mussel adhesive protein-coated titanium oxide  
403 nanoparticles for effective NO removal from versatile substrates, *Chem. Eng. J.* 378  
404 (2019) 122164.
- 405 [15] M.S. Azmina, R. Md Nor, H.A. Rafeie, N.S.A. Razak, S.F.A. Sani, Z. Osman, Enhanced  
406 photocatalytic activity of ZnO nanoparticles grown on porous silica microparticles, *Appl.*  
407 *Nanosci.* 7 (2017) 885-892.
- 408 [16] H.-R. Lim, H.S. Kim, R. Qazi, Y.-T. Kwon, J.-W. Jeong, W.-H. Yeo, Advanced Soft  
409 Materials, Sensor Integrations, and Applications of Wearable Flexible Hybrid Electronics  
410 in Healthcare, Energy, and Environment, *Adv. Mater.* 32 (2020) 1901924.
- 411 [17] C.-T. Lee, Y.-S. Wang, High-performance room temperature  $\text{NH}_3$  gas sensors based on  
412 polyaniline-reduced graphene oxide nanocomposite sensitive membrane, *J. Alloys.*  
413 *Compd.* 789 (2019) 693-696.
- 414 [18] C. Liu, H. Tai, P. Zhang, Z. Ye, Y. Su, Y. Jiang, Enhanced ammonia-sensing properties  
415 of PANI-TiO<sub>2</sub>-Au ternary self-assembly nanocomposite thin film at room temperature,  
416 *Sens. Actuator B Chem.* 246 (2017) 85-95.
- 417 [19] N. Tang, C. Zhou, L. Xu, Y. Jiang, H. Qu, X. Duan, A Fully Integrated Wireless Flexible  
418 Ammonia Sensor Fabricated by Soft Nano-Lithography, *ACS Sens.* 4 (2019) 726-732.
- 419 [20] L. Du, D. Feng, X. Xing, C. Wang, Y. Gao, S. Sun, G. Meng, D. Yang, Nanocomposite-  
420 Decorated Filter Paper as a Twistable and Water-Tolerant Sensor for Selective Detection  
421 of 5 ppb–60 v/v% Ammonia, *ACS Sens.* 7 (2022) 874-883.
- 422 [21] X. Sun, R. Gao, Y. Wu, X. Zhang, X. Cheng, S. Gao, Y. Xu, L. Huo, Novel in-situ  
423 deposited  $\text{V}_2\text{O}_5$  nanorods array film sensor with enhanced gas sensing performance to n-  
424 butylamine, *Chem. Eng. J.* 459 (2023) 141505.
- 425 [22] N. Panahi, M. Shirazi, M.T. Hosseinejad, Fabrication, characterization and hydrogen

- 426 gas sensing performance of nanostructured V<sub>2</sub>O<sub>5</sub> thin films prepared by plasma focus  
427 method, *J. Mater. Sci. Mater. El.* 29 (2018) 13345-13353.
- 428 [23] A. Moretti, S. Passerini, Bilayered Nanostructured V<sub>2</sub>O<sub>5</sub>·nH<sub>2</sub>O for Metal Batteries, *Adv.*  
429 *Energy Mater.* 6 (2016) 1600868.
- 430 [24] Q. Sun, H. Cheng, Y. Yuan, Y. Liu, W. Nie, K. Zhao, K. Wang, W. Yao, X. Lu, J. Lu,  
431 Uncovering the Fundamental Role of Interlayer Water in Charge Storage for Bilayered  
432 V<sub>2</sub>O<sub>5</sub> · nH<sub>2</sub>O Xerogel Cathode Materials, *Adv. Energy Mater.* 13 (2023) 2202515.
- 433 [25] K. Zhou, Y. He, Q. Xu, Q.e. Zhang, A.a. Zhou, Z. Lu, L.-K. Yang, Y. Jiang, D. Ge, X.Y.  
434 Liu, H. Bai, A Hydrogel of Ultrathin Pure Polyaniline Nanofibers: Oxidant-Templating  
435 Preparation and Supercapacitor Application, *ACS Nano* 12 (2018) 5888-5894.
- 436 [26] K. Momma, F. Izumi, VESTA3 for three-dimensional visualization of crystal, volumetric  
437 and morphology data, *J. Appl. Cryst.* 44 (2011) 1272-1276.
- 438 [27] C. Xiong, A.E. Aliev, B. Gnade, K.J. Balkus, Fabrication of Silver Vanadium Oxide and  
439 V<sub>2</sub>O<sub>5</sub> Nanowires for Electrochromics, *ACS Nano* 2 (2008) 293-301.
- 440 [28] H. Zhang, X. Han, R. Gan, Z. Guo, Y. Ni, L. Zhang, A facile biotemplate-assisted  
441 synthesis of mesoporous V<sub>2</sub>O<sub>5</sub> microtubules for high performance asymmetric  
442 supercapacitors, *Appl. Surf. Sci.* 511 (2020) 145527.
- 443 [29] Z. Zhao, X. Wang, X. Jing, Y. Zhao, K. Lan, W. Zhang, L. Duan, D. Guo, C. Wang, L.  
444 Peng, X. Zhang, Z. An, W. Li, Z. Nie, C. Fan, D. Zhao, General Synthesis of Ultrafine  
445 Monodispersed Hybrid Nanoparticles from Highly Stable Monomicelles, *Adv. Mater.* 33  
446 (2021) 2100820.
- 447 [30] F. Qu, S. Zhang, C. Huang, X. Guo, Y. Zhu, T. Thomas, H. Guo, J.P. Attfield, M. Yang,  
448 Surface Functionalized Sensors for Humidity-Independent Gas Detection, *Angew. Chem.*  
449 *Int. Ed.* 60 (2021) 6561-6566.
- 450 [31] P. Guo, B. Tian, J. Liang, X. Yang, G. Tang, Q. Li, Q. Liu, K. Zheng, X. Chen, W. Wu,  
451 An All-Printed, Fast-Response Flexible Humidity Sensor Based on Hexagonal-WO<sub>3</sub>  
452 Nanowires for Multifunctional Applications, *Adv. Mater.* (2023) 2304420.
- 453 [32] K. Suematsu, M. Sasaki, N. Ma, M. Yuasa, K. Shimano, Antimony-Doped Tin Dioxide  
454 Gas Sensors Exhibiting High Stability in the Sensitivity to Humidity Changes, *ACS Sens.*  
455 1 (2016) 913-920.
- 456 [33] D. Feng, L. Du, X. Xing, C. Wang, J. Chen, Z. Zhu, Y. Tian, D. Yang, Highly Sensitive  
457 and Selective NiO/WO<sub>3</sub> Composite Nanoparticles in Detecting H<sub>2</sub>S Biomarker of  
458 Halitosis, *ACS Sens.* 6 (2021) 733-741.
- 459 [34] B. Zhang, L. Wang, Y. Zhang, Y. Ding, Y. Bi, Ultrathin FeOOH Nanolayers with  
460 Abundant Oxygen Vacancies on BiVO<sub>4</sub> Photoanodes for Efficient Water Oxidation,  
461 *Angew. Chem. Int. Ed.* 57 (2018) 2248-2252.
- 462 [35] B. Tong, Z. Deng, B. Xu, G. Meng, J. Shao, H. Liu, T. Dai, X. Shan, W. Dong, S. Wang,  
463 S. Zhou, R. Tao, X. Fang, Oxygen Vacancy Defects Boosted High Performance p-Type  
464 Delafossite CuCrO<sub>2</sub> Gas Sensors, *ACS Appl. Mater. Interfaces* 10 (2018) 34727-34734.

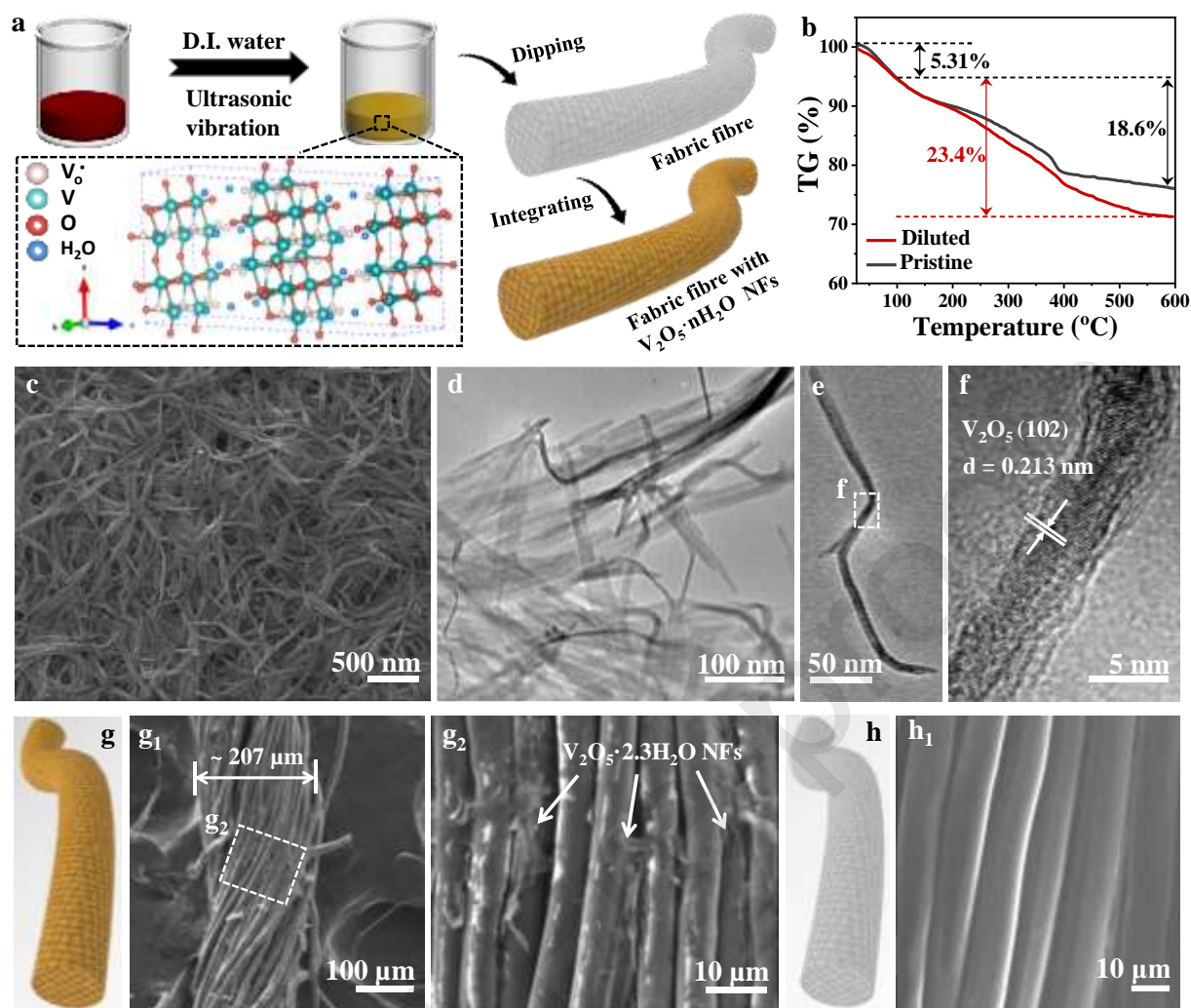


- 465 [36] K. Schneider, M. Lubecka, A. Czapla,  $V_2O_5$  thin films for gas sensor applications, *Sens.*  
466 *Actuator B Chem.* 236 (2016) 970-977.
- 467 [37] D. Yao, C. Dong, Q. Bing, Y. Liu, F. Qu, M. Yang, B. Liu, B. Yang, H. Zhang, Oxygen-  
468 Defective Ultrathin  $BiVO_4$  Nanosheets for Enhanced Gas Sensing, *ACS Appl. Mater.*  
469 *Interfaces* 11 (2019) 23495-23502.
- 470 [38] X. Xing, L. Du, D. Feng, C. Wang, M. Yao, X. Huang, S. Zhang, D. Yang, Individual gas  
471 sensor detecting dual exhaled biomarkers via a temperature modulated n/p  
472 semiconducting transition, *J. Mater. Chem. A* 8 (2020) 26004-26012.
- 473 [39] L. Xu, C. Wang, X. Zhang, D. Guo, Q. Pan, G. Zhang, S. Wang,  $NO_x$  sensitivity of  
474 conductometric  $In(OH)_3$  sensors operated at room temperature and transition from p- to  
475 n- type conduction, *Sens. Actuator B Chem.* 245 (2017) 533-540.
- 476 [40] H. Wu, J. Yu, G. Yao, Z. Li, W. Zou, X. Li, H. Zhu, Z. Huang, Z. Tang, Room temperature  
477  $NH_3$  sensing properties and humidity influence of  $Ti_3C_2T_x$  and  $Ag-Ti_3C_2T_x$  in an oxygen-  
478 free environment, *Sens. Actuator B Chem.* 369 (2022) 132195.
- 479 [41] D. Wang, D. Zhang, Y. Yang, Q. Mi, J. Zhang, L. Yu, Multifunctional  
480 Latex/Polytetrafluoroethylene-Based Triboelectric Nanogenerator for Self-Powered  
481 Organ-like MXene/Metal–Organic Framework-Derived  $CuO$  Nanohybrid Ammonia  
482 Sensor, *ACS Nano* 15 (2021) 2911-2919.
- 483 [42] Y. Liu, H. Ji, Z. Yuan, H. Zhu, L. Kong, H. Gao, F. Meng, Hollow urchin  $Co-Fe_2O_3$  with  
484 outstanding selectivity and fast responding for ppb level  $NH_3$  sensing via Lewis acid-base  
485 effect, *Chem. Eng. J.* 474 (2023) 145620.
- 486 [43] K.-P. Yuan, L.-Y. Zhu, J.-H. Yang, C.-Z. Hang, J.-J. Tao, H.-P. Ma, A.-Q. Jiang, D.W.  
487 Zhang, H.-L. Lu, Precise preparation of  $WO_3@SnO_2$  core shell nanosheets for efficient  
488  $NH_3$  gas sensing, *J. Colloid Interf. Sci.* 568 (2020) 81-88.
- 489 [44] F. Ranjbar, S. Hajati, M. Ghaedi, K. Dashtian, H. Naderi, J. Toth, Highly selective  
490 MXene/ $V_2O_5/CuWO_4$ -based ultra-sensitive room temperature ammonia sensor, *J. Hazard.*  
491 *Mater.* 416 (2021) 126196.
- 492 [45] D. Maity, R.T.R. Kumar, Polyaniline Anchored MWCNTs on Fabric for High  
493 Performance Wearable Ammonia Sensor, *ACS Sens.* 3 (2018) 1822-1830.
- 494 [46] D. Lv, W. Shen, W. Chen, R. Tan, L. Xu, W. Song, PSS-PANI/PVDF composite based  
495 flexible  $NH_3$  sensors with sub-ppm detection at room temperature, *Sens. Actuator B*  
496 *Chem.* 328 (2021) 129085.
- 497 [47] D. Zhang, Y. Yang, Z. Xu, D. Wang, C. Du, An eco-friendly gelatin based triboelectric  
498 nanogenerator for a self-powered PANI nanorod/ $NiCo_2O_4$  nanosphere ammonia gas  
499 sensor, *J. Mater. Chem. A* 10 (2022) 10935-10949.
- 500 [48] X. Wang, D. Zhang, H. Zhang, L. Gong, Y. Yang, W. Zhao, S. Yu, Y. Yin, D. Sun, In  
501 situ polymerized polyaniline/MXene ( $V_2C$ ) as building blocks of supercapacitor and  
502 ammonia sensor self-powered by electromagnetic-triboelectric hybrid generator, *Nano*  
503 *Energy* 88 (2021) 106242.
- 504 [49] Y. Fu, T. Wang, X. Wang, X. Li, Y. Zhao, F. Li, G. Zhao, X. Xu, Investigation of p-n

505 sensing transition and related highly sensitive  $\text{NH}_3$  gas sensing behavior of SnPx/rGO  
506 composites, Chem. Eng. J. 471 (2023) 144499.

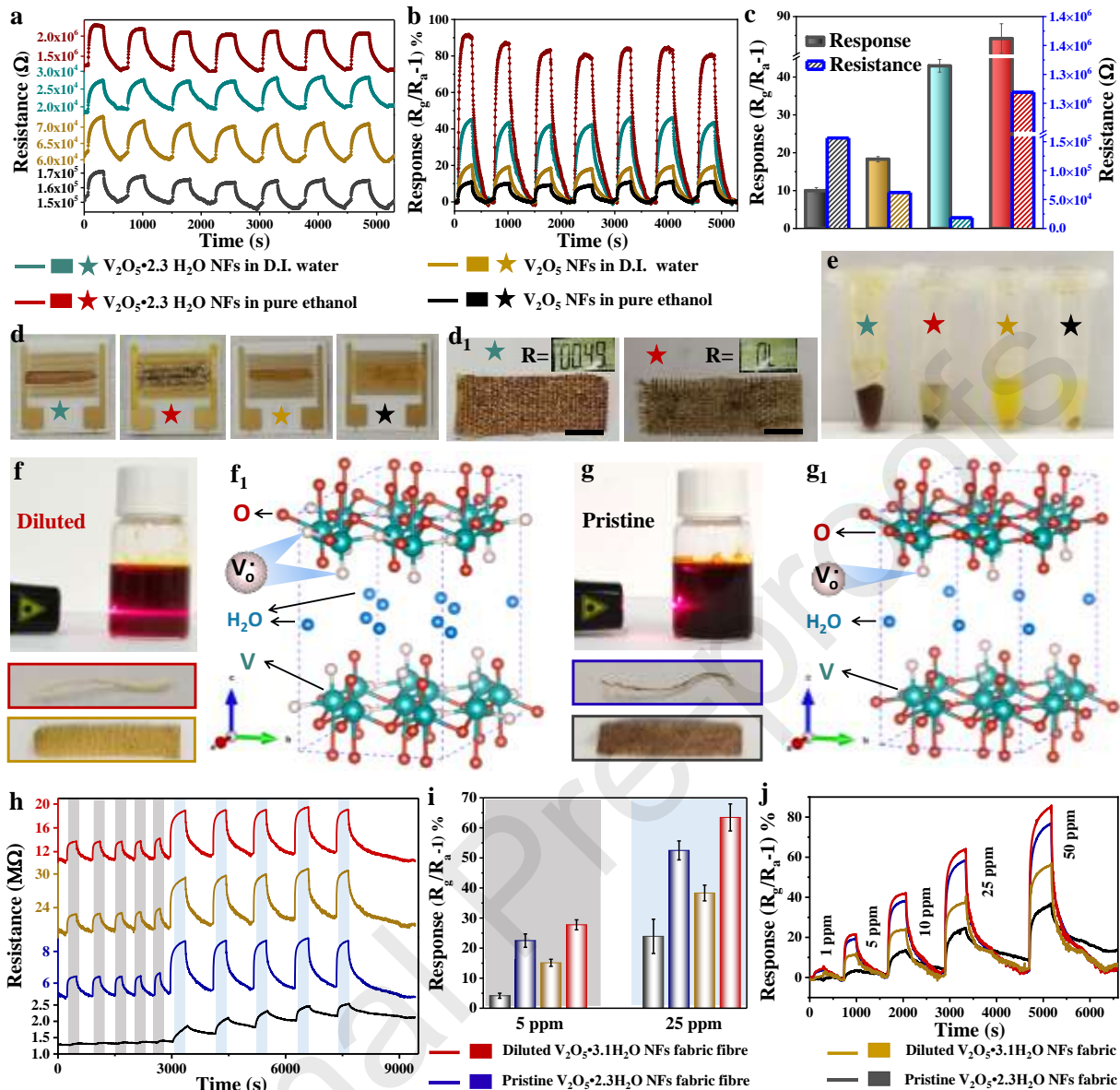
507

Journal Pre-proofs



508

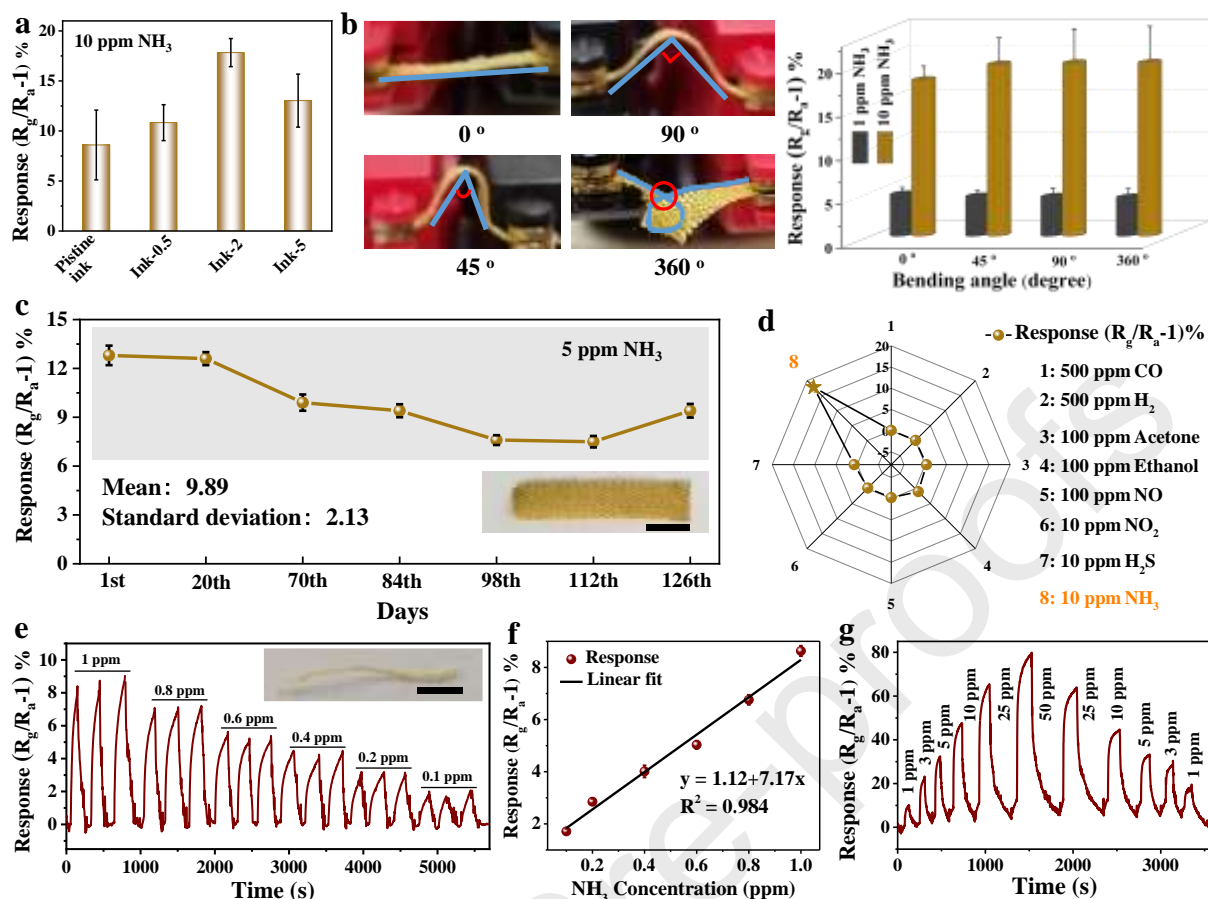
509 **Fig. 1.** The synthesis and characterization of V<sub>2</sub>O<sub>5</sub>·nH<sub>2</sub>O NFs. (a) The schematic diagram of  
 510 diluting and integrating V<sub>2</sub>O<sub>5</sub>·nH<sub>2</sub>O NFs ink, and the simulated crystal structure of V<sub>2</sub>O<sub>5</sub>·nH<sub>2</sub>O  
 511 NFs. (b) The TGA curves of pristine and diluted V<sub>2</sub>O<sub>5</sub>·nH<sub>2</sub>O NFs. (c) The SEM, (d-e) TEM  
 512 and (f) HRTEM images of pristine V<sub>2</sub>O<sub>5</sub>·2.3H<sub>2</sub>O NFs. (g) The schematic diagram and (g<sub>1</sub>-g<sub>2</sub>)  
 513 SEM images of fabric fiber integrated with V<sub>2</sub>O<sub>5</sub>·nH<sub>2</sub>O NFs ink. (h) The schematic diagram  
 514 and (h<sub>1</sub>) the SEM image of bare fabric fiber.



515

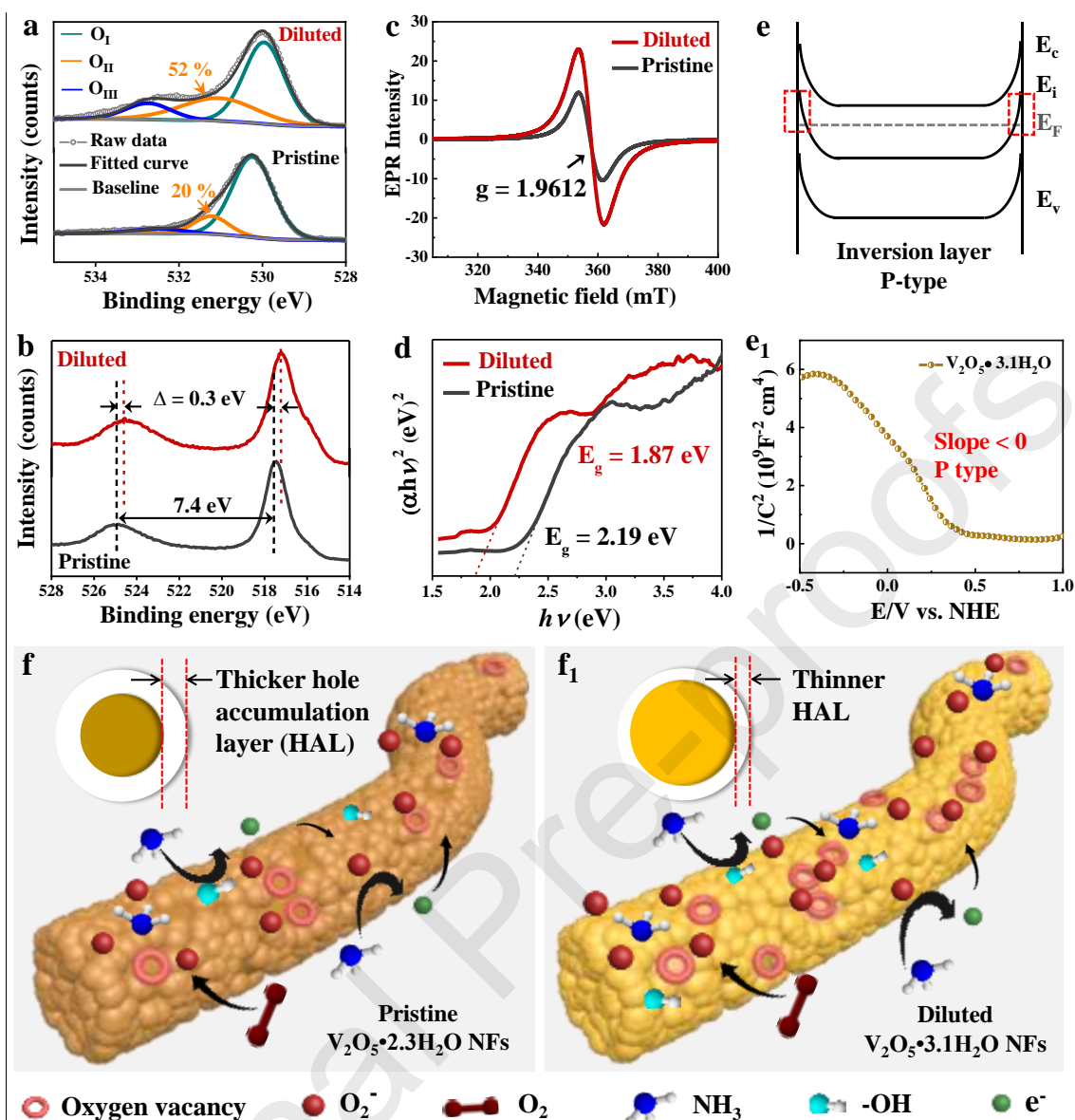
516 **Fig. 2.** The NH<sub>3</sub> sensing comparison between freeze-dried and annealed V<sub>2</sub>O<sub>5</sub>·2.3H<sub>2</sub>O NFs  
 517 powder being dispersed in D.I. water and pure ethanol, respectively. (a) The real-time resistance  
 518 and (b) sensing curves to 10 ppm NH<sub>3</sub>, and corresponding (c) histogram of baseline resistance  
 519 and response value. (e) The photograph of above four dispersions and (d) integrated interdigital  
 520 electrode. (d<sub>1</sub>) The freeze-dried V<sub>2</sub>O<sub>5</sub>·2.3H<sub>2</sub>O NFs dispersed in D.I. water and pure ethanol  
 521 were integrated onto the fabric, respectively. The scale bars in (d<sub>1</sub>) are 0.5 cm. The photographs  
 522 and structures of (f-f<sub>1</sub>) diluted and (g-g<sub>1</sub>) pristine V<sub>2</sub>O<sub>5</sub>·nH<sub>2</sub>O NFs inks. The “Tyndall effect”  
 523 of diluted V<sub>2</sub>O<sub>5</sub>·3.1H<sub>2</sub>O NFs ink irradiated by red light ( $\lambda = 638$  nm). The comparison on NH<sub>3</sub>  
 524 sensing performance between diluted and pristine V<sub>2</sub>O<sub>5</sub>·nH<sub>2</sub>O NFs inks integrated on fabric  
 525 and the fabric fibre, respectively. (h) The real-time resistance curves and (i) the summarized  
 526 responses. (j) The response curves to various NH<sub>3</sub> concentration. The RH of (a-b, h-j) is at ~  
 527 22%.





528

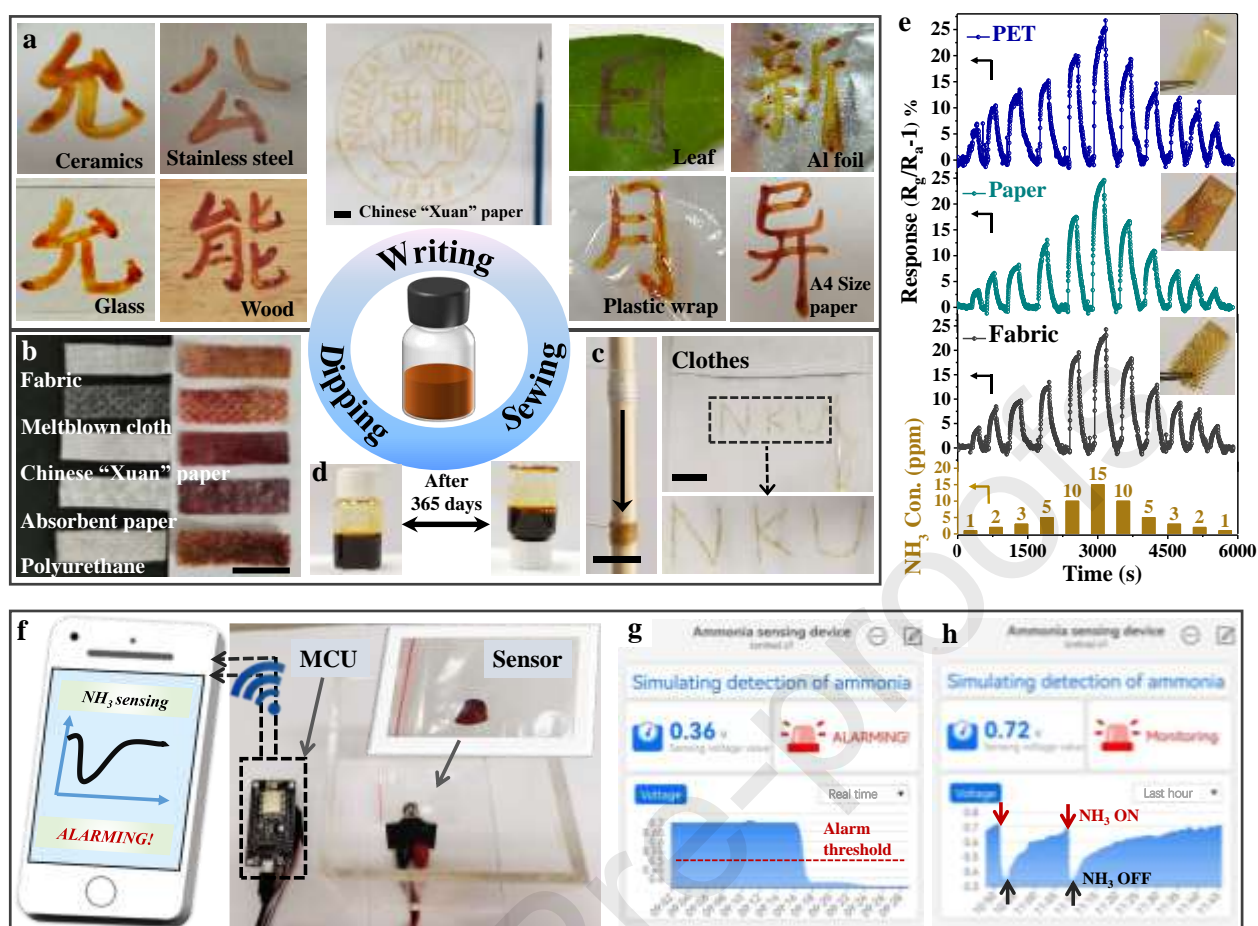
529 **Fig. 3.** The systematic NH<sub>3</sub> sensing evaluation of V<sub>2</sub>O<sub>5</sub>·nH<sub>2</sub>O NFs ink integrated over fabrics:  
 530 (a) The dilution-dependent sensing response of V<sub>2</sub>O<sub>5</sub>·nH<sub>2</sub>O NFs ink, (b) the V<sub>2</sub>O<sub>5</sub>·3.1H<sub>2</sub>O NFs  
 531 fabric under various bending angle and their corresponding sensing responses, (c) the long-term  
 532 stability and (d) selectivity of diluted V<sub>2</sub>O<sub>5</sub>·3.1H<sub>2</sub>O NFs fabric. The NH<sub>3</sub> sensing evaluation of  
 533 V<sub>2</sub>O<sub>5</sub>·3.1H<sub>2</sub>O NFs fabric fiber: (e) The response curve to 0.1-1 ppm NH<sub>3</sub>, (f) the relationship  
 534 between sensing responses and NH<sub>3</sub> concentrations, (g) the response curve to various NH<sub>3</sub>  
 535 concentrations. The scale bars in (c) and (e) are 0.5 cm. The RH of (a-b, d, e-g) is at ~ 19% and  
 536 RH of (c) is at ~ 19%-57%.



537

538 **Fig. 4.** The various characterizations on oxygen vacancy of pristine  $V_2O_5 \cdot 2.3H_2O$  NFs and  
 539 diluted  $V_2O_5 \cdot 3.1H_2O$  NFs. High-resolution XPS spectra are related to (a) O 1s and (b) V 2p,  
 540 (c) EPR spectra and (d) plots of  $(\alpha h\nu)^2$  vs photon energy ( $h\nu$ ). The schematic energy-band  
 541 variation of  $V_2O_5 \cdot nH_2O$  NFs. (e) An inversion layer marked with red rectangle and p-type  
 542 surface conductivity. (e₁) The Mott-Schottky plot of  $V_2O_5 \cdot 3.1H_2O$  NFs. The  $NH_3$  sensing  
 543 mechanism diagrams of (f) pristine  $V_2O_5 \cdot 2.3H_2O$  NFs and (f₁) diluted  $V_2O_5 \cdot 3.1H_2O$  NFs.

544



545

546 **Fig. 5.** The universal substrates-tolerant and multi means-integratable  $\text{NH}_3$  sensing. (a) The  
 547  $\text{V}_2\text{O}_5 \cdot 2.3\text{H}_2\text{O}$  NFs ink for drawing the school badge and the motto of Nankai University onto  
 548 hard and flexible substrates. (b) The pristine  $\text{V}_2\text{O}_5 \cdot 2.3\text{H}_2\text{O}$  ink was evenly integrated onto  
 549 various flexible substrates as examples. (c) The diluted  $\text{V}_2\text{O}_5 \cdot 3.1\text{H}_2\text{O}$  NFs ink integrated fabric  
 550 fiber for sewing patterns into clothes. (d) The photographs of  $\text{V}_2\text{O}_5 \cdot 3.1\text{H}_2\text{O}$  NFs ink after  
 551 storing 365 days. (e) The  $\text{NH}_3$  sensing of diluted  $\text{V}_2\text{O}_5 \cdot 3.1\text{H}_2\text{O}$  NFs ink integrated on flexible  
 552 substrates with PET, Chinese "Xuan" paper and fabric as examples, and "Con." in the ordinate  
 553 represents concentration. The scale bars in (a, b, c) are all 1 cm. (f) Simulated detection of  $\text{NH}_3$   
 554 were conducted by intergrating the  $\text{V}_2\text{O}_5 \cdot 3.1\text{H}_2\text{O}$  NFs ink onto sample bag and communicating  
 555 with a smartphone. (g) Smartphone reading the real-time sensing parameters and the records of  
 556 alarming to 10 ppm  $\text{NH}_3$  and (h) the historical measurements. The RH of (e) is at  $\sim 22\%$ .

557 **Table 1.** Comparison of various NH<sub>3</sub> sensing materials in both presenting forms and NH<sub>3</sub>  
558 sensing.

Material type	Materials	Presenting forms	Substrates	Mechanical flexibility	Integrating means	W T <sup>a)</sup>	Response@Con. <sup>c)</sup>	T <sub>res</sub> /T <sub>rec</sub> time (s) @ Con. <sup>c)</sup>	LOD <sup>b)</sup> (ppm)	Refs. <sup>b)</sup>
	Co-Fe <sub>2</sub> O <sub>3</sub>	powder	ceramic tube	No	spin-coating combined with calcination	275 °C	275% <sup>d)</sup> @10 ppm	7.2/5.4@10 ppm	0.01 <sup>d)</sup>	[42]
	MoO <sub>3</sub> nanorods	powder	glass	No	spin-coating by mixing with solvent	200 °C	36% <sup>d)</sup> @5 ppm	230/267@5 ppm	~5 <sup>d)</sup>	[8]
	WO <sub>3</sub> @SnO <sub>2</sub> Core nanosheet shell	thin film	MEMS	No	dripping-coating by mixing with solvent	200 °C	1.5 <sup>e)</sup> @15 ppm	62/42@15 ppm	5 <sup>d)</sup>	[43]
SMOs based NH <sub>3</sub> sensing materials	Ni-doped nanostructure	In <sub>2</sub> O <sub>3</sub> powder	ceramic tube	No	coating by mixing with solvent	140 °C	2732 ppm <sup>e)</sup> @50 ppm	23/10@50 ppm	~1 <sup>d)</sup>	[9]
	MXene/CuO composite.	solution	epoxy	Yes	spraying	RT	24.8 <sup>d)</sup> @100 ppm	43/26@100 ppm	~1 <sup>d)</sup>	[41]
	MXene/V <sub>2</sub> O <sub>5</sub> /CuWO <sub>4</sub>	precipitate	alumina sheet with interdigitated gold electrode	No	coating	RT	53.5 <sup>d)</sup> @51 ppm	1.6/4@51 ppm	1 <sup>d)</sup> 0.3 <sup>d)</sup>	[44]
	V <sub>2</sub> O <sub>5</sub> -nH <sub>2</sub> O NFs	ink	ceramics, stainless steel, glass, wood, paper, leaf, Al foil, plastic wrap, fabric and polyurethane	Yes	dripping, writing, dipping and sewing	RT <sup>b)</sup>	~4.2% ppm <sup>e)</sup> @1 ppm	75/36@1 ppm	~0.1 <sup>d)</sup>	This work
Carbon based NH <sub>3</sub> sensing	PANI/MWCNTs	-	polypropylene fabric	Yes	spray-coating and chemical polymerization	RT	61.54% ppm <sup>e)</sup> @20 ppm	9/30@20 ppm	0.2 <sup>d)</sup>	[45]

materials											
PEDOT:PSS nanowires	aqueous suspension	PET	Yes	spin-coating	RT	~2.2% ppm	<sup>g)</sup> @6	96/318@6 ppm	0.1 <sup>j)</sup>	[19]	
PSS-PANI/PVDF	-	PVDF membrane	Yes	in-situ polymerization	RT	70% <sup>g)</sup> @1 ppm		160/400@1 ppm	~ 0.1 <sup>i)</sup>	[46]	
Pt-NDs/PPy-nanolayer@CNTs	powder	filter paper	Yes	coating by mixing with solvent	RT	~40% <sup>g)</sup> ppm	@50	2/~10@2 v/v%	~0.005 <sup>j)</sup>	[20]	
PANI/NiCo <sub>2</sub> O <sub>4</sub>	powder	gelatin film	Yes	spin-coating	RT	4.67 <sup>f)</sup> @20 ppm		22/62@20 ppm	~ 0.5 <sup>i)</sup>	[47]	
PANI/MXene	solution	epoxy	Yes	dripping	RT	27% <sup>g)</sup> @5 ppm		27/5@5 ppm	~ 0.3 <sup>i)</sup>	[48]	
SnPx/rGO	powder	interdigitated electrodes	No	dripping	RT	117.5% <sup>d)</sup> to 40 ppm		126/306@10 ppm	0.0436 <sup>j)</sup>	[49]	

559 <sup>a)</sup> Working temperature, <sup>b)</sup> Room temperature, <sup>c)</sup> Concentration, <sup>d)</sup> Calculated by  $(R_a/R_g - 1) * 100\%$ , <sup>e)</sup> Calculated by  $R_a/R_g$ , <sup>f)</sup> Calculated by  $R_g/R_a$ , <sup>g)</sup> Calculated by  $(R_g/R_a - 1) * 100\%$ , <sup>h)</sup>  
560 Limit of Detection, <sup>i)</sup> Experimental measurements, <sup>j)</sup> Theoretical calculation, <sup>k)</sup> References.  
561

562

563 **Declaration of interests**

564

565  The authors declare that they have no known competing financial interests or personal  
566 relationships that could have appeared to influence the work reported in this paper.

567

568  The authors declare the following financial interests/personal relationships which may be  
569 considered as potential competing interests:

570

571

572

573

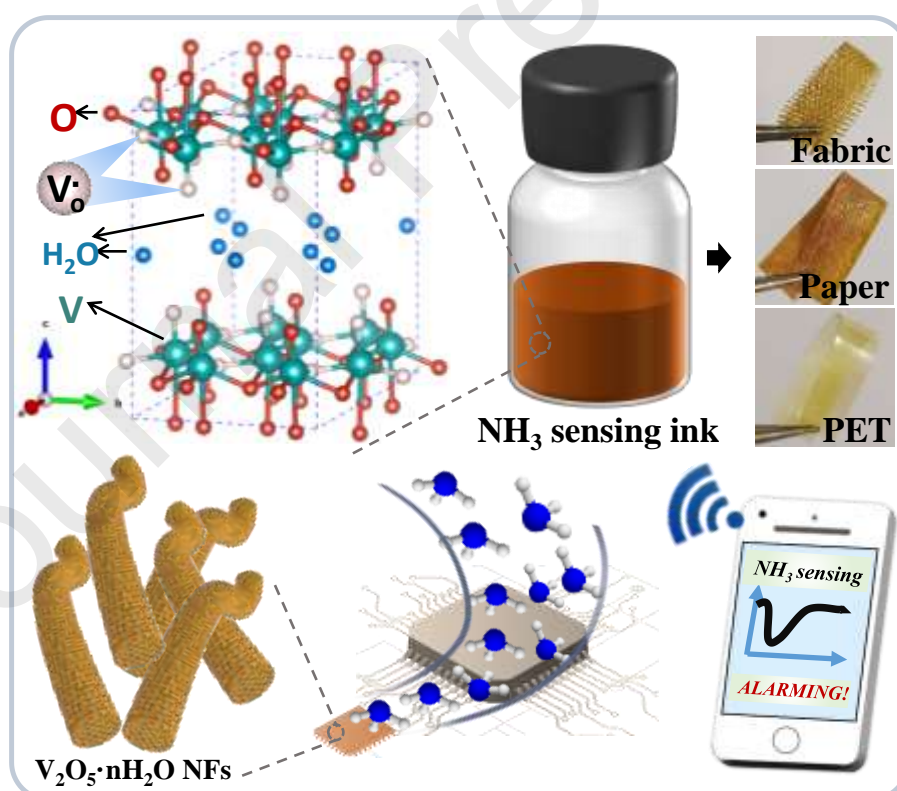
574

575

576

577

## Graphical Abstracts



578

579

580

581

## Highlights

1. The excellent dispersed and stable  $\text{V}_2\text{O}_5 \cdot 3.1\text{H}_2\text{O}$  nanofibers ink has been developed.

- 582 2. The ink toward universal substrates-tolerant and multi means-integratable  $\text{NH}_3$  sensing.
- 583 3. The oxygen vacancy governed  $\text{NH}_3$  sensing mechanism is rationally interpreted.
- 584 4. Simulation on detecting  $\text{NH}_3$  is conducted with reliable sensing response.
- 585

Journal Pre-proofs